Journal of the European Ceramic Society 20 (2000) 2767–2772

www.elsevier.com/locate/jeurceramsoc

# Improved chemical stability of ZnO–BaO based varistors

A.C. Caballero *, F.J. Valle, M. Villegas, C. Moure, P. Durán, J.F. Fernández

*Department of Electroceramics, Instituto de Cerámica y Vidrio, CSIC, 28500 Arganda del Rey, Madrid, Spain*

**Abstract**

Non-linear current–voltage response of ZnO–BaO based ceramic materials makes them valuable for varistors manufacturing. Although this behaviour is quantitatively similar to that observed in the binary ZnO–$Bi_2O_3$ system, their commercial use is limited because the BaO rich secondary phase is severely damaged by moisture due to its high solubility in water. In the present work, doping with $P_2O_5$ to form $BaZn_2(PO_4)_2$ and $Zn_3(PO_4)_2$ has been studied in order to improve the resistance of ZnO–BaO materials to degradation by moisture. The water solubility of sintered samples has been evaluated by lixiviation experiments. Sintering behaviour and microstructure development have been followed by dilatometry and microstructure was analysed by scanning electron microscopy. The electrical properties of these materials evidence varistor behaviour with non-linearity values similar to those observed for binary materials ZnO–BaO and ZnO–$Bi_2O_3$. 

*Keywords:* ZnO varistors; Chemical stability

## 1. Introduction

It is well known that ZnO based ceramic materials doped with different oxides exhibit non-linear current–voltage (*I–V*) responses (varistor behaviour) and are able to bear high energy transients. In fact ZnO ceramics are widely used for varistor manufacturing. Commercial compositions are based on the ZnO–$Bi_2O_3$ and ZnO–$Pr_6O_{11}$ systems and also include other dopant oxides. Manufactured varistors for applications as surge arresters are mostly based on the ZnO–$Bi_2O_3$ system.[1]

The varistor behaviour originates in the microstructure of the ceramic. The basic microstructure to obtain non-linear *I–V* response can be summarised as semiconducting ZnO grains surrounded by an insulating Bi-rich phase. The non-linearity is observed in ZnO–ZnO grain junctions showing either a thin Bi-rich layer or the presence of segregated $Bi^{3+}$ cations. According to the Double Schottky Barrier model, potential barriers are formed at these grain boundaries which govern the electrical properties of the ceramic. This kind of microstructure can be obtained by doping with an oxide of very low solubility in ZnO, which is segregated to the ZnO grain boundaries. Varistor effect has been reported to occur in ZnO based materials doped with cations of large ionic radius.[2,3]

Materials based on ZnO–BaO show great potential for varistor applications. Previous works on binary materials of the ZnO–BaO system[4,5] have reported dense ceramic materials with non-linear coefficients larger than those observed in binary ZnO–$Bi_2O_3$ ceramics. On the other hand, the BaO-rich phase located at grain boundaries and triple points is highly soluble in water and favours the material degradation by moisture. This leads to severe damage of the electrical properties of the materials and even to structural damage if they are simply stored in air. Therefore, improving the resistance of these materials to attack by moisture is critical to consider their use for commercial varistors manufacturing.

According to the phase diagram of the ZnO–BaO–$P_2O_5$ ternary system,[6] the incorporation of a certain amount of phosphorous can lead to the formation of $BaZn_2(PO_4)_2$ and $Ba_3(PO_4)_2$ or $Zn_3(PO_4)_2$; depending on the relative amounts of BaO and $P_2O_5$ the composition would lie in one of the two compatibility triangles determined by ZnO–$BaZn_2(PO_4)_2$–$Ba_3(PO_4)_2$ or ZnO–$BaZn_2(PO_4)_2$–$Zn_3(PO_4)_2$, none of these phases exhibit significant solubility in water.[7] Therefore, avoiding the presence of BaO, the material would not be dramatically affected by moisture.

The incorporation of phosphorous in ceramic $BaTiO_3$ has been reported to control the microstructure development of the material. Furthermore, $Ba_3(PO_4)_2$ can form at temperatures of the order of 900°C, playing a

* Corresponding author. Tel.: +9-91-871180; fax: +9-91-8700550.
*E-mail address:* amador@icv.csic.es (A.C. Caballero).

0955-2219/00/$ - see front matter 
PII: S0955-2219(00)00226-0

key role on the final microstructure and changing the electrical properties of the material.[8,9]

In the present work, we have studied the incorporation of $P_2O_5$ to a ZnO–BaO material in order to improve its stability against moisture while keeping its varistor properties. Microstructure development, sintering behaviour and the electrical *I–V* characteristic curves have been analysed.

## 2. Experimental procedure

### 2.1. Sample preparation and characterisation

Samples were prepared from ZnO, $BaCO_3$ and ester phosphate. ZnO (Merck 8849) shows an average particle size of 2 μm and >99% purity. Barium was incorporated from $BaCO_3$ (Merck 1712) with 1.7 μm average particle size and >99% purity. The phosphorous precursor was ester phosphate (Merck 820251) which is actually composed of 60% di-ester phosphate and 40% monoester phosphate. Its characteristics are reported elsewhere.[8]

Appropriate amounts of ZnO and $BaCO_3$ were dispersed in a solution of ester phosphate in isopropyl alcohol by means of a high speed turbine (6000 rpm). The dispersion was oven dried below 100°C and the powder was sieved through a 100 μm mesh. Green compacts were obtained by isostatic pressing at 200 MPa. The sintering behaviour was analysed from the shrinkage curves obtained by dilatometry. According to these curves, certain temperatures were selected for isothermal sintering, which was carried out for 2 h. For both isothermal and constant heating rate sintering, the heating and cooling rates were 3°/min. The crystalline phases present in the sintered material were determined by X-ray diffraction (XRD). Ground samples were scanned at 1°2θ/min. The microstructure was analysed by scanning electron microscopy (SEM) on polished surfaces. Average grain size was estimated from SEM micrographs by the interception method.

Electrical measurements were made on 1.5 mm thick sintered discs electroded with silver. The *I–V* curves were obtained for d.c. signals and the non-linearity coefficient was calculated for currents densities between 1 and 10 mA/cm$^2$.

### 2.2. Lixiviation experiments and chemical analysis

The water solubility of the phases present in the sintered material has been studied by aqueous lixiviation experiments for the three cations included in the material (Ba, P and Zn). The procedure proposed by Bennett and Red[10] to determine the presence of water-soluble salts in clays and refractories has been followed. The material is ground in an agate mortar to obtain powder below 100 μm. A suspension of 1.00 g of this material in 50 ml of distilled water is prepared in a polyethylene jar by magnetic stirring for 60 min. Once the solid is decanted, the solution is filtered through a double fine pore paper (ALBET 242). The filtered solution was diluted to 100 ml being ready for analysis.

Chemical analysis has been done on dried powders and sintered samples. The later were ground in an agate mortar. Both samples with a similar particle size to that of the lixiviation experiments are taken into solution by etching with HCl (1 + 1).

Phosphorous, Barium and Zinc contents have been determined by inductively coupled plasma (ICP) (Jobin-Yvon JY-38-VHR). The analytic lines selected were the most sensitive reported in the literature.[11] The ionic line Ba II 455.403 nm and the atomic lines P I 214.914 nm and Zn I 213.856 nm were found free of interference. Spectral background caused by the acidic attack of the samples has been corrected by using standards with blank reactivities according to the acidity used for sample dissolution. This correction is not necessary for the case of aqueous lixiviation.

Table 1
Chemical analysis (wt.%) of the dried powder, sintered material (1200°C) and aqueous lixiviated

| Component | Dried powder | Material sintered at 1200°C | Lixiviated | MCD[a] in the lixiviated |
|---|---|---|---|---|
| BaO | 0.27 | 0.28 | 0.0013 | 0.00080 |
| $P_2O_5$ | 0.36 | 0.32 | <0.0050 | 0.0050 |
| ZnO | 99.37 | 99.40 | 0.0095 | 0.0010 |

[a] MCD, minimum concentration detectable.

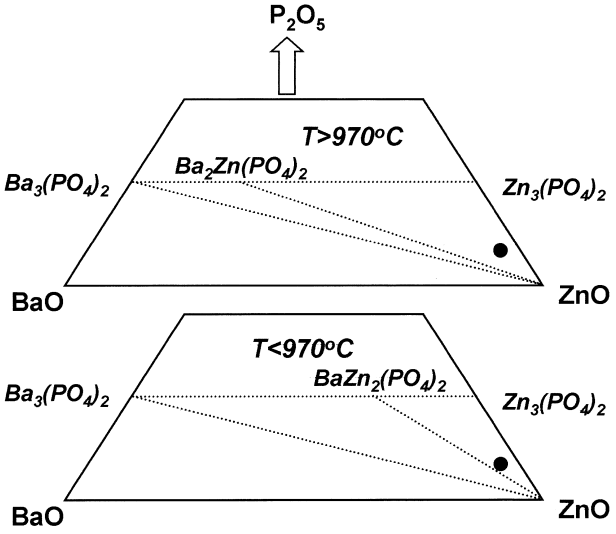


Fig. 1. Compatibility triangles for the ZnO-rich region of the ZnO–BaO–$P_2O_5$ system for high and low temperature according to Ref. 6. Sample composition is marked with a black circle.

Multi-element standards (Ba, P, and Zn) were prepared in de-mineralized water and (P and Ba) in HCl with concentration ranges which cover the amounts detected on the analysed samples. The analysis of the lixiviate has been extended to the three cations under study; however, chemical analysis of the material composition has only been done on P and Ba. Since the ZnO is the main component, its concentration has been calculated by subtracting the measured concentration from the other two constituents.

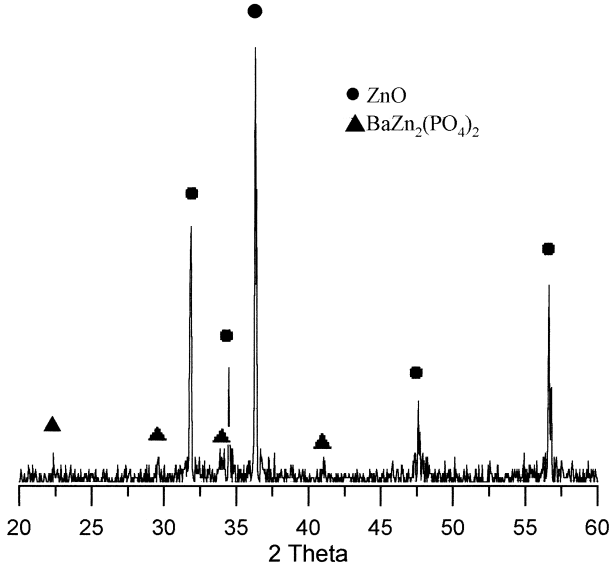


Fig. 2. X-ray powder diffraction pattern of the sample sintered at 1200°C.

## 3. Results and discussion

### 3.1. Composition and crystalline phases

The results of the chemical analysis for the dried powder, sintered samples and lixiviated samples are summarised in Table 1. The phosphorous concentration measured for the sintered samples is slightly lower than that of the dried powder. This points to phosphorous volatilisation during the sintering process. However, in spite of this loss, the composition of both the dried powder and the sintered material lie within the compatibility triangle $ZnO–BaZn_2(PO_4)_2–Zn_3(PO_4)_2$ of the $ZnO–BaO–P2O_5$ system[6] (Fig. 1). Fig. 2 shows the powder diffraction pattern of the sample sintered at 1200°C. Two crystalline phases are clearly detected: ZnO (JCPDF 36-1451) and $BaZn_2(PO_4)_2$ (JCPDF 16-554), the expected $Zn_3(PO_4)_2$ concentration is well

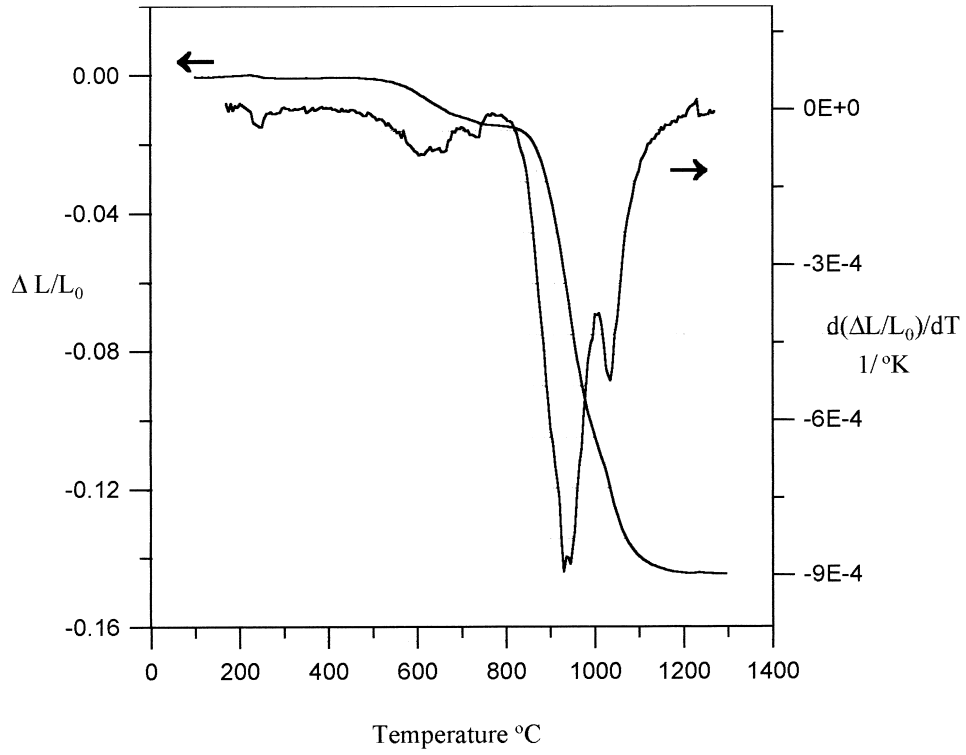


Fig. 3. Shrinkage and shrinkage rate curves as a function of temperature.

below 1%, which is under the detection limit of this technique. The results of the lixiviation experiments discard the presence of BaO (composition shift to the $ZnO–BaZn_2(PO_4)_2–BaO$ compatibility triangle), since this phase is highly soluble in water, its presence should be associated with a large Ba concentration measured in the lixiviated material. This is not the case of the samples analysed.

Consequently with the extremely low solubility in water of the phases present in the sintered material, the resistance to degradation by moisture is greatly improved. This is evidenced by the results of the chemical analysis of the lixiviated material: the lixiviated BaO concentration is less than 0.5% of the total BaO amount, and the lixiviated concentration of all the components is less than 1% of their total amount.

### 3.2. Sintering behaviour and microstructure development

Shrinkage and shrinkage rate curves up to 1300°C are shown in Fig. 3. Shrinkage takes place between 500 and 1200°C. The shrinkage rate curve shows three different regions: up to 800°C, between 800 and 1000°C showing the maximum shrinkage rate at 910°C, and a third region which extends to 1200°C. The burn out of the ester phosphate organic chain takes place at temperatures below 500°C, therefore it does not contribute to the shape of the measured shrinkage curve. On the other hand, $BaCO_3$ decomposition may affect to the shrinkage observed at the initial sintering stage; however, the magnitude of the shrinkage observed and the low $BaCO_3$ concentration indicates that the shrinkage measured is mainly due to the beginning of sintering. For isothermal sintering, the apparent density of the samples show a sharp increase (Fig. 4) when the sintering temperature is increased from 1000 to 1050°C. For sintering temperatures ranging between 1050 and 1200°C, the apparent density value of the samples remains constant between 96 and 98% of the theoretical ZnO density. According to previously reported results,[12] for materials in the system ZnO–BaO sintering occurs in the presence of liquid phase. Furthermore, the binary system $ZnO–P_2O_5$ shows an eutectic point around 1000°C,[13] therefore it seems that the rapid densification increase observed between 800 and 1000°C is the consequence of a liquid phase sintering mechanism.

SEM micrographs of the samples sintered at 1050 and 1150°C (Fig. 5) show that extensive grain growth occurs

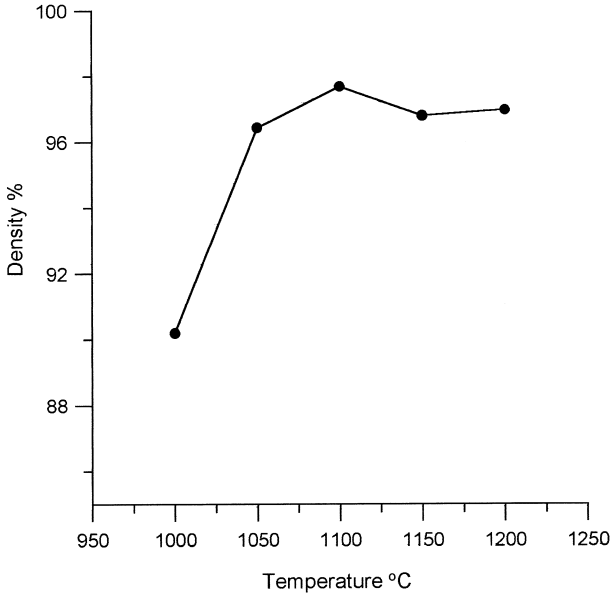


Fig. 4. Apparent density for different sintering temperatures (2 h soaking time).

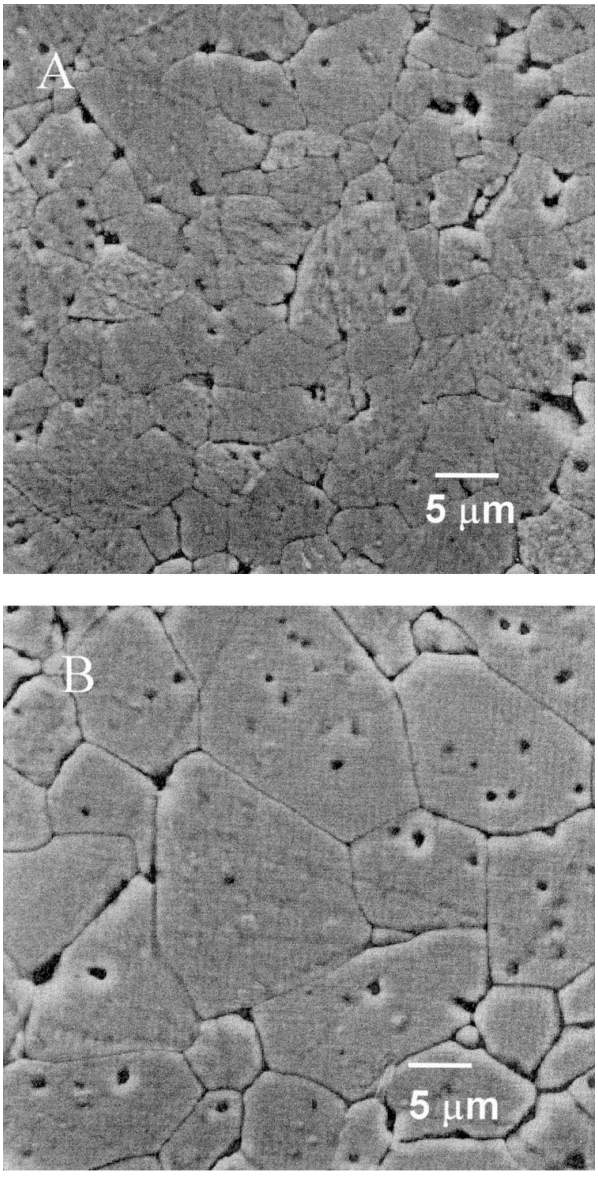


Fig. 5. SEM micrographs on polished and etched surfaces of samples sintered at (a) 1050°C and (b) 1150°C.

Table 2
Average grain size, non-linearity coefficient and electric field for samples sintered at different temperatures

| Sintering temperature (°C) | Average grain size (μm) | Non-linearity coefficient $\alpha$ | Electric field at 1 mA/cm$^2$ (V/cm) |
|---|---|---|---|
| 1050 | 6±0.5 | 2 | 930 |
| 1100 | 10±0.5 | 4 | 520 |
| 1150 | 15±0.5 | 5 | 330 |
| 1200 | 19±0.5 | 7 | 180 |

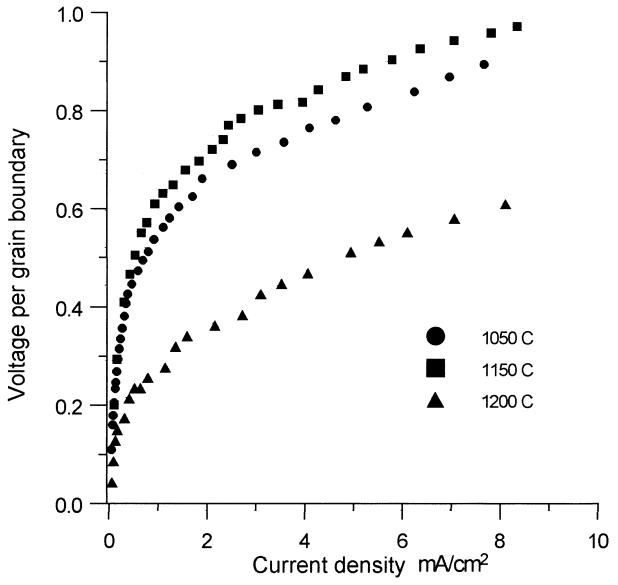


Fig. 6. *I–V* curves (normalised per grain boundary) for samples sintered at different temperatures.

when increasing the sintering temperature. Although the apparent density of these samples remains unchanged, the average grain size increase from 6 μm for the sample sintered at 1050°C to 19 μm for the sample sintered at 1200°C (Table 2).

### 3.3. Electrical characterisation

According to the data presented in Table 2, the decrease of the breakdown voltage measured for the samples sintered at higher temperatures is directly related with the larger average grain size. Since the non-linear *I–V* response of the material originates at the grain boundaries, for samples with the same thickness the number of grain boundaries decrease when increasing the grain size.[3] Nevertheless, consequently with the lower sintering temperatures needed for these materials, their microstructure exhibit finer grains than binary ZnO–BaO materials[5] which allows them to reach higher breakdown voltages.

The non-linearity coefficient α (Table 2) increases with the sintering temperature. For the sample sintered at 1200°C the calculated $\alpha$-value is 7, which is comparatively high when compared to value of 3 reported for a ZnO–BaO binary material containing twice the BaO concentration in the materials of the present work.

Fig. 6 shows the *I–V* response normalised per grain boundary, where the number of grain boundaries is calculated from the sample thickness and the average grain size. These curves seem to indicate that the grain boundary potential barrier height is lower for the samples sintered at 1200°C; however this is in disagreement with the higher $\alpha$-value measured for these samples. The contradiction between these results can be understood if the calculated number of grain boundaries does not coincide with the electrically active grain boundaries. In fact not all the grain boundaries are electrically active,[3] and the calculated *I–V* curve for the sample sintered at 1200°C seems to point to an overestimation of the number of electrically active boundaries.

## 4. Conclusions

The incorporation of $P_2O_5$ to ZnO–BaO materials avoids the presence of BaO rich phases with high solubility in water and leads to the formation of $BaZn_2(PO_4)_2$ and $Zn_3(PO_4)_2$ with low solubility in water. Lixiviation experiments carried out on sintered samples have shown its high resistance to attack by water. For sintering temperatures ranging from 1050 to 1200°C the apparent density remains constant around 97% of the theoretical ZnO density and extensive grain growth is observed when increasing the sintering temperature. The non-linearity coefficient α measured for the material sintered at 1200°C is higher than that reported for a binary ZnO–BaO material containing twice the BaO concentration incorporated in the materials of the present work.

## Acknowledgements

This work has been supported by the CICYT projects MAT97-0694-C02-01 and PETRI 95-0364-OP.

## References

1. Einzinger, R., Metal oxide varistors. *Annu. Rev. Mater. Sci.*, 1987, **17**, 299–321.
2. Matsuoka, M., Nonohmic properties of zinc oxide ceramics. *Jpn J. Appl. Phys.*, 1971, **10**(5), 736–746.
3. Greuter, F., Electrically active interfaces in ZnO varistors. *Sol. State Ionics*, 1995, **75**, 67–78.
4. Bhushan, B., Kashyap, S. C. and Chopra, K. L., Novel nonohmic binary composite. *Appl. Phys. Lett.*, 1981, **38**(3), 160–161.
5. Fan, J. and Freer, R., Varistor properties and microestructure of ZnO–BaO ceramics. *J. Mater. Sci.*, 1997, **32**, 415–419.

6. Hoffman, M. V., The systems BaO–MgO–$P_2O_5$ and BaO–ZnO–$P_2O_5$: compounds and fluorescence. *J. Electrochem. Soc.*, 1963, **110**(12), 1223–1227.
7. *Handbook of Chemistry and Physics*. 46th edn. 1965–1966. The Chemical Rubber Co., Cleveland, OH.
8. Caballero, A. C., Fernández, J. F., Durán, P. and Moure, C., Efecto de la incorporación de fósforo en la microestructura y propiedades eléctricas del $BaTiO_3$ cerámico. *Bol. Soc. Esp. Ceram. Vidr.*, 1993, **32**(3), 169–174.
9. Caballero, A. C., Fernández, J. F., Durán, P. and Moure, C., Phosphor-doped $BaTiO_3$: microstructure development and dielectric properties. *J. Mater. Sci.*, 1995, **30**, 3799–3804.
10. Benett, H. and Reed, R. A., *Chemical Methods of Silicate Analysis*. The British Ceramic Research Association/Academic Press, London, 1971.
11. Boumans, P. W. J. M. (ed.), *Inductively Coupled Plasma Emission Spectroscopy*. Wiley–Interscience, New York, 1987.
12. Uematsu, K., Terada, A., Morimoto, T., Uchida, N. and Saito, K., Direct determination of grain growth behavior in zinc oxide with added barium oxide. *J. Am. Ceram. Soc.*, 1989, **72**(6), 1070–1072.
13. Nordand, A. G. and Kierkegaard, P., Crystal chemistry of some anhydrous divalent-metal phosphates. *Chem. Script*, 1980, **15**, 27–39.